

Mechanistic Aspects of Propene Epoxidation by Hydrogen Peroxide. Catalytic Role of Water Molecules, External Electric Field, and Zeolite Framework of TS-1

Jernej Stare,^{†,‡,§} Neil J. Henson,[†] and Juergen Eckert^{*,‡,||}

Theoretical Division and Los Alamos Neutron Science Center, Los Alamos National Laboratory, New Mexico 87545, National Institute of Chemistry, Hajdrihova 19, SI-1000 Ljubljana, Slovenia, and Materials Research Laboratory, University of California, Santa Barbara, California 93106

Received July 8, 2008

We have assessed various aspects of the epoxidation of propene by hydrogen peroxide, a reaction of considerable industrial importance, and elucidated some of the important factors that govern its mechanism. Quantum chemical calculations on the reactants, products, and transition states were performed both in the gas phase and using models to represent the TS-1 (titanosilicalite-1) catalyst. The reaction energy for the uncatalyzed process is computed as -52.6 kcal/mol with a barrier of 35.2 kcal/mol in the gas phase using the B3LYP hybrid density functional and a 6-31+G(d,p) basis set. The reaction appears to occur via a concerted mechanism. The competing reaction of ionic addition of hydrogen peroxide to the double bond to form a hydroperoxopropene is computed to have a reaction energy of only -17.1 kcal/mol with a barrier of 34.8 kcal/mol and is therefore expected not to be thermodynamically preferable. Introduction of water molecules to the model is calculated to reduce the reaction barrier to 25.7 kcal/mol in the case of a single molecule but did not significantly affect the reaction energy. The competing addition reaction barrier appears to be significantly less sensitive to the presence of water molecules, suggesting that the concerted epoxidation reaction is also kinetically favored in the polar environment. Introduction of additional water molecules does not result in a noticeable enhancement. The water molecules appear to mediate proton transfer between the peroxide oxygens in the rate determining step of the concerted epoxidation reaction. The introduction of a background solvent field was also found to reduce the activation energy. For example, a model with a single explicit water molecule and the solvent field gives an activation barrier of 16.9 kcal/mol. A similar effect is observed if an external electric field is applied to the model with the dipole component directed along the O–O bond direction. Calculations were also performed on the same reaction occurring in the vicinity of a model for the active site of the TS-1 catalyst using a cluster model. The activation barrier for the cluster model is calculated to be 25.8 kcal/mol with a reaction energy of -55.5 kcal/mol, which is comparable to the gas phase model with a single water molecule added. No significant changes are observed with the addition of water molecules in this model.

1. INTRODUCTION

Titanium silicalite-1 (TS-1) is a highly selective catalyst used primarily in the epoxidation of alkenes and the hydroxylation of phenol and linear alkanes with hydrogen peroxide with water as the benign byproduct.^{1,2} TS-1 is a crystalline microporous solid with the silicalite (MFI) zeolite framework that features interconnected straight and sinusoidal channels of molecular dimensions. The framework structure consists of an array of corner sharing SiO₄ tetrahedra where approximately 2.6% of the silicon T-sites are isomorphously substituted by titanium. The key structural question, which bears on the origin of the unique catalytic properties of this material, is that of whether the titanium substitution is random or if some of the twelve crystallographically inequivalent T-sites are more likely to contain Ti than others. This question has been of intense interest to both

experimentalists and theoreticians. There have been several diffraction experiments to address this issue, both synchrotron X-ray and neutron diffraction studies, including the use of isotopic substitution to improve scattering contrast.^{3–5} The problem has also received significant attention from theoreticians. The most recent work in this area have been a study using an embedded quantum mechanical approach by Rösch and co-workers⁶ and probably the most definitive studies using fully periodic Hartree–Fock⁷ and DFT methods.⁸ These studies often produced conflicting predictions, although several showed distinct preferences for the T(8) and T(10) sites.

The oxidation chemistry with titanosilicalite catalysts and other related materials has proved to be a fruitful topic for experimental and theoretical studies of reaction mechanisms.⁹ A recent review by Lamberti and co-workers highlighted the importance of the close synergy between experiment and theory to fully elucidate the subtleties in this system.¹⁰ Earlier work from the same group in collaboration with others has provided a very detailed picture of titanium hydroperoxo linkages in the catalytic mechanism.¹¹ Baiker and co-workers have addressed the issue of representing the TS-1 structure with a finite cluster model of titanium silsesquioxanes as

* To whom correspondence should be addressed. E-mail: juergen@mrl.ucsb.edu.

[†] Theoretical Division, Los Alamos National Laboratory.

[‡] Los Alamos Neutron Science Center, Los Alamos National Laboratory.

[§] National Institute of Chemistry, Slovenia.

^{||} Materials Research Laboratory, University of California.

soluble models of the active site.¹² Wells and co-workers¹³ performed a DFT study on the reactivity of TS-1 active sites and concluded that the catalytic activity is promoted by Si-vacancies adjacent to the Ti sites. The role of hydrolysis in the formation of the TS-1 active sites has been elaborated by Sokol and co-workers.¹⁴ Studies of similar catalytic materials for propene epoxidation included various related systems, for example the gold–titanium catalyst in which the processes of absorption and desorption of propene and epoxide species to and from the surface of the catalyst are believed to be essential parts of the catalytic mechanism.¹⁵ A considerable amount of work has been devoted to various aspects of the epoxidation of small olefins and alcohols by a variety of oxidizing agents. Theoretical studies of these reactions included a number of catalytic compounds or environments such as fluorinated alcohols,¹⁶ dioxiranes,^{17,18} vanadyl cation,¹⁹ cytochrome P450,²⁰ and metallic silver surface.²¹ Crehuet and co-workers have explored the reactivity of ethylene toward some small reactive organic oxide species by highly accurate CASPT2, CCSD(T), and DFT methods.²² The long standing problem of the local structure and reaction mechanisms in heterogeneous catalysts has also given rise to the development of novel computational approaches, particularly development of force fields²³ and embedding techniques.^{24–27} Embedding models have been tested on the example of proton transfer in zeolites and yielded results of comparable reliability as the constrained cluster models, yet at lower costs.²⁸ Recently Wells and co-workers published a concise comparative study of five distinct previously proposed catalytic mechanisms of propene epoxidation with TS-1 as catalyst.²⁹ They calculated the activation free energies for propene epoxidation by using various forms of reactive species involving the TS-1 active site represented as a gas-phase cluster treated by DFT model chemistry. Their findings suggest that the hydrolyzed site defect structure of the TS-1 active site with dangling silanol and titanol groups provides the most effective catalytic pathway among the mechanisms under consideration.

In this paper, we present a detailed theoretical investigation of the prototypical epoxidation reaction of propene with hydrogen peroxide in the presence of water molecules. Our calculations were aimed at assessing the effect of the environment on the catalytic reaction, and were therefore performed using various models for the TS-1 active site in addition to baseline gas phase calculations. Part of the present study is closely related to the work of Wells and co-workers²⁹ in that both consider the same mechanism of propene epoxidation in the presence of a TS-1 active site modeled as a cluster. However, as the focus of our study is to assess various physical conditions that influence the epoxidation reaction rather than to compare a variety of possible mechanisms, it is to be viewed as complementary to this earlier work.

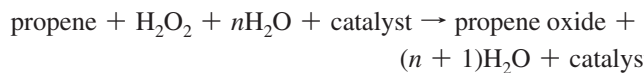
2. METHODS AND MODELS

Quantum chemical calculations were performed on models for the epoxidation of propene by hydrogen peroxide in the gas phase, as well as various types of environment, such as a continuum solvation model, uniform dipolar electric field, and the internal surface of a titanium-substituted silicalite

zeolite pore. All calculations were performed using the *Gaussian 03* software.³⁰

We used the B3LYP hybrid density functional^{31,32} along with the 6–31+G(d,p) basis set for the quantum chemical calculations. Test calculations showed that for most of the structural and vibrational properties, as well as for reaction energetics, the results obtained with the use of this basis set readily converged with respect to the size of the basis set up to the 6–311++G(2d,2p) level. We also tested the MP2 ab initio method for the structures of species involved in propene epoxidation and for the reaction energetics. While optimized MP2 structures were fairly similar to those obtained by B3LYP, a steady offset in reaction energy and activation barrier was observed, with the MP2 energies being by about 7–8 kcal/mol more negative and barriers lower by about 2–3 kcal/mol. These differences were, however, nearly insensitive to the modeling of the environment. Because the primary focus of this work was the relative changes of reaction parameters upon changing the type of modeling, we therefore used the less expensive B3LYP method in our calculations.

Because the actual catalytic reaction proceeds in the presence of water in a zeolite cavity, it is important to include water molecules in the calculations as well as a representation of the active surface of the zeolite catalyst. In a real system the presence of a considerable number of water molecules is always given because the oxidant hydrogen peroxide is introduced as a solution with at least two water molecules per one H₂O₂ molecule. The reaction in the presence of *n* water molecules and the catalyst can therefore be written as



n was typically varied from 0 to 2, but in some cases, up to *n* = 5 water molecules were included in our model. Although water molecules may be considered as “spectators” in the propene epoxidation reaction, their interaction with reactive species and transition states can alter the reaction mechanism and thereby result in a catalytic role of water. A detailed study on this aspect is given in section 3.1.

The major part of the present work consists of the geometry optimization of the structures of reactants (R), products (P), and transition states (TS) for various types of models ranging from the bare reacting propene and H₂O₂ molecules to the large-scale quantum mechanics/molecular mechanics (QM/MM) model of the zeolite channel. Geometry optimizations were performed using the Berny analytical gradient method and were further verified by the calculation of harmonic frequencies. Solvent effects (section 3.3) were assessed using water with the self-consistent reaction field (SCRF) method based on the integral equation formalism of the polarizable continuum model (IEPCM), as developed by Tomasi and co-workers³³ and implemented into the *Gaussian 03* program package. Transition state searches were performed to determine optimal mechanisms for the catalytic conversion of sorbate molecules. It was found that standard QST2 and QST3 search algorithms were ineffective for the models proposed here, mainly because of the large structural differences between R, TS, and P. Scans along a suitably chosen coordinate were performed to provide approximate starting models for TS structures, which could then be further

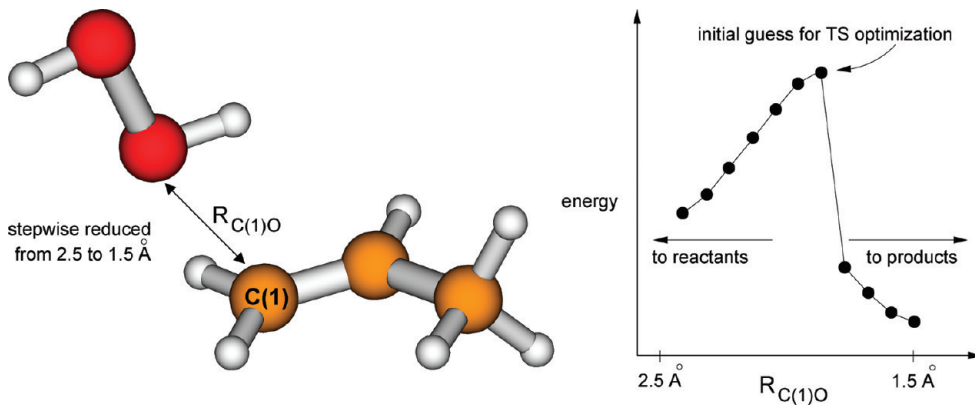


Figure 1. Determination of an initial guess for the transition state. Left: The approach between propene and hydrogen peroxide is controlled by the $C(1)\cdots O$ distance. Right: Energy profile along the $R_{C(1)O}$ coordinate; the structure corresponding to the highest point in the energy profile is used as the initial guess for the transition state geometry optimization.

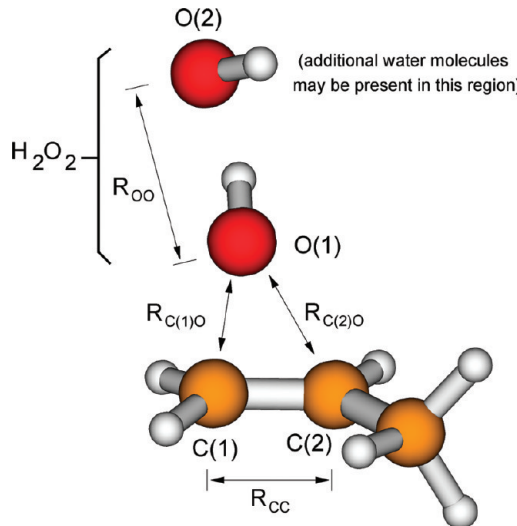


Figure 2. Atom labels and selected metric parameters of the propene epoxidation transition state.

refined using standard methods (Figure 1). A similar approach for locating the transition state was also used for alternative reaction mechanisms (section 3.2). Transition states were characterized by selected geometric parameters (Figure 2), harmonic vibrational analysis, as well the calculation of atomic charges and bond-antibond stabilization interactions via natural bond orbital analysis.^{34,35} Details on this approach are given in section 3.1.

All the epoxidation reactions considered in this work were assumed to take on a concerted polar character rather than a radical one. Test open-shell TS optimization for $n = 0$ yields the same results as the restricted calculation, and the energy of the TS in a triplet electronic state is notably higher than the one of the singlet state. Configuration interaction calculations also indicate no notable difference in the amount of higher electronic states in the correlated wavefunctions of R, P, and TS—in all cases, the wavefunction was found to be over 90% of the HF ground-state character. It is therefore reasonable to proceed with the polar mechanism of the propene epoxidation reaction.

For the epoxidation reaction in the gas phase, two possible mechanisms of the nonradical mediated process are suggested by elementary organic chemistry, which may be classified as Markovnikov and anti-Markovnikov. In agreement with previous findings,¹⁶ several isomers of transition states were

found for the propene epoxidation reaction. These differ in the location of the $C=C$ bond initially approached by the O(1) of hydrogen peroxide. Transition states of Markovnikov type are generally more stable, but the differences with anti-Markovnikov isomers were found to be very small, that is, they did not exceed 0.8 kcal/mol between the lowest and the highest energy isomer. Moreover, these differences between isomers become less pronounced, both in structural and energetic terms, as n is increased. The reason for this trend is that the O(1) of the incoming H_2O_2 molecule tends to be farther away from the propene molecule and thus more nearly equidistant from C(1) and C(2), which in turn smears out differences between Markovnikov and anti-Markovnikov structures of the transition state. Unless otherwise stated, all results reported in section 3 therefore correspond to the Markovnikov type of reaction mechanism, as is reflected in the fact that $R_{C(1)O} < R_{C(2)O}$. In section 3.2, we also consider a possible alternative reaction that may take place between propene and H_2O_2 in the gas phase, namely, the concerted polar addition of H_2O_2 to the propene double bond.

It is widely assumed that the strong electrostatic field present in the pores of the zeolite structure is one of the factors that promotes their catalytic properties. We have attempted to investigate this effect by applying an external dipole electric field to the gas phase models and align it along a coordinate of interest. This is detailed in section 3.4.

To assess the influence on the propene epoxidation of the explicit interactions established within the TS-1 catalyst, we constructed several cluster representations of zeolite models. There are two independent crystallographic structure determinations of the TS-1 structure both of which used combined refinements of X-ray and neutron diffraction data from powder samples.^{3,4} We used the results of Hijar and co-workers, who showed that titanium is located in a nonrandom substitution pattern in the silicalite structure, as basis for the construction of the zeolite models. The following methodology was used to assemble the cluster models. Hijar and co-workers found that the site with the highest probability for titanium substitution is T(8), so that this site serves as the starting point for building our clusters. Clusters of different sizes are then constructed from this central point in such a way as to progressively include more coordination shells of silicon atoms taken from the original TS-1 structure as shown in Figure 3. Atoms that lie in the interior of the zeolite pore structure and are therefore inaccessible to sorbate

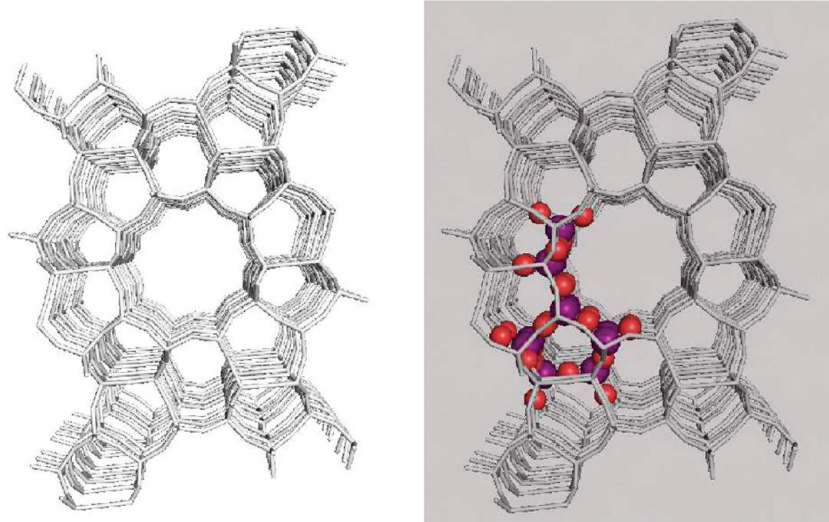


Figure 3. Construction of the clusters. Left: Crystal structure of TS-1. Right: Cluster is built up extending from the Ti site and incorporating adjacent SiO_4 tetrahedra.

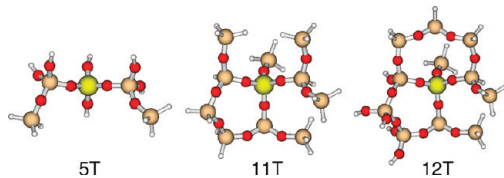


Figure 4. Three different QM cluster models used for the representation of the TS-1 active site.

molecules were excluded from the cluster model. At the periphery of the model, the clusters were terminated by hydrogen atoms to saturate the spare valences on silicon or oxygen atoms; Si–H and O–H termination bonds were used and the positions of the terminal hydrogens were aligned along the respective Si–O bond directions as given by crystallography to enforce the constraints of the crystal framework. The corresponding terminal Si–H and O–H distances were frozen to values obtained with a B3LYP/6–31+G(d,p) geometry optimization of free SiH_4 and $\text{Si}(\text{OH})_4$ molecules, respectively, that is, to 1.484807 Å for Si–H and 0.96189 Å for O–H. Clusters of several shapes and sizes were constructed in this manner, and their geometry was optimized under the constraints outlined above. At this preliminary stage, the B3LYP/6–31+G(d,p) level of theory was used. Three such clusters (5T, 11T, and 12T) are displayed on Figure 4. With a total number of 53 atoms, the 12T cluster was at the upper size limit for “affordable” model systems.

The selection of the cluster to be employed for the modeling of the catalyzed epoxidation reaction mechanism was carried out on the basis of the convergence of geometric parameters with the cluster size, particularly those involving the central TiO_4 tetrahedron. We found that larger clusters provided notably higher flexibility about the titanium active site, which resulted in large increase of the accessible space to sorbate molecules at the Ti site. While binding energies of water and hydrogen peroxide were somewhat less affected by the cluster size, binding of hydroperoxy anion was significantly stronger in the large, flexible cluster than in a smaller and more rigid one (Table 1). We found that a reasonable convergence of calculated structure and binding energies was achieved with the 11T cluster shown on Figure

Table 1. Counterpoise-Corrected B3LYP/6-31+G(d,p) Binding Energies (in kcal/mol) of Water, Hydrogen Peroxide, and Hydroperoxy Anion to Three Different Clusters (5T, 11T, 12T, Figure 4) Representing the Active Site of TS-1

ligand	cluster		
	5T	11T	12T
H_2O	4.5	9.4	10.1
H_2O_2	7.5	8.1	6.6
OOH^-	39.2	96.0	89.0

4, and therefore, we chose this particular cluster for the ensuing calculations of the reaction mechanism. Note that this cluster contains only one terminal hydride of the Si–H type. In addition we determined that a simplified basis set can be used with this cluster, which only marginally alters its calculated properties, namely, 6–31G(d,p) basis functions on the central $\text{Ti}(\text{OSi})_4$ moiety, 6–31G on the other non-hydrogen atoms, and STO-3G on the terminal hydrogens. The choice of the minimal basis functions for the terminal hydrogens is based on the fact that such a basis set makes them effectively more electronegative (and thus more similar to the oxygen atoms which they replace), as has been pointed out in previous studies.³⁶ All molecules interacting with the zeolite model (water, hydrogen peroxide, propene) were treated with the 6–31G(d,p) basis set.

3. RESULTS AND DISCUSSION

3.1. Gas-Phase Model: Catalytic Role of Water Molecules. The most significant parameters which characterize the reaction and the corresponding transition state are summarized in Table 2 as a function of the number of additional water molecules (up to 5) surrounding the propene– H_2O_2 reaction complex. An explanation of the metric parameters is given in Figure 2. The reaction energy (ΔE) does not appear to depend significantly on the value of n . The difference between the least and the most negative value is relatively small (5.5 kcal/mol), and there is no uniform trend in ΔE as function of n . The reason for this is most likely the fact that the potential energy surface of the surrounding water cluster is very flat and contains several minima. This makes it likely that the water molecules can

Table 2. Gas-Phase B3LYP/6-31+G(d,p) Propene Epoxidation Reaction Energy (ΔE) and Barrier (ΔE^\ddagger) (both in kcal/mol), Selected Metric Parameters of the Transition State (in Å), the Imaginary Transition State Harmonic Frequency (ν^\ddagger , in cm^{-1}), and Natural Charges of Selected Atoms, Calculated with Different Number of Additional Water Molecules (n) in the Model^a

n	ΔE	ΔE^\ddagger	$R_{\text{C}(1)\text{O}}$	$R_{\text{C}(2)\text{O}}$	R_{OO}	R_{CC}	ν^\ddagger	natural charge			
								O(1)	O(2)	C(1)	C(2)
0	-52.6	35.2	1.677	2.235	1.979	1.403	509	-0.599	-0.823	-0.276	-0.115
1	-57.0	25.7	1.757	2.191	1.949	1.392	448	-0.581	-0.850	-0.290	-0.100
2	-53.2	24.2	1.840	2.114	1.945	1.386	439	-0.576	-0.877	-0.308	-0.072
3	-51.5	25.8	1.911	2.128	1.912	1.380	431	-0.574	-0.885	-0.325	-0.074
4	-52.9	25.1	1.952	2.093	1.902	1.378	430	-0.575	-0.879	-0.327	-0.081
5	-53.6	25.1	2.002	2.040	1.895	1.377	426	-0.572	-0.875	-0.329	-0.087

^a See Fig. 2 for explanation.

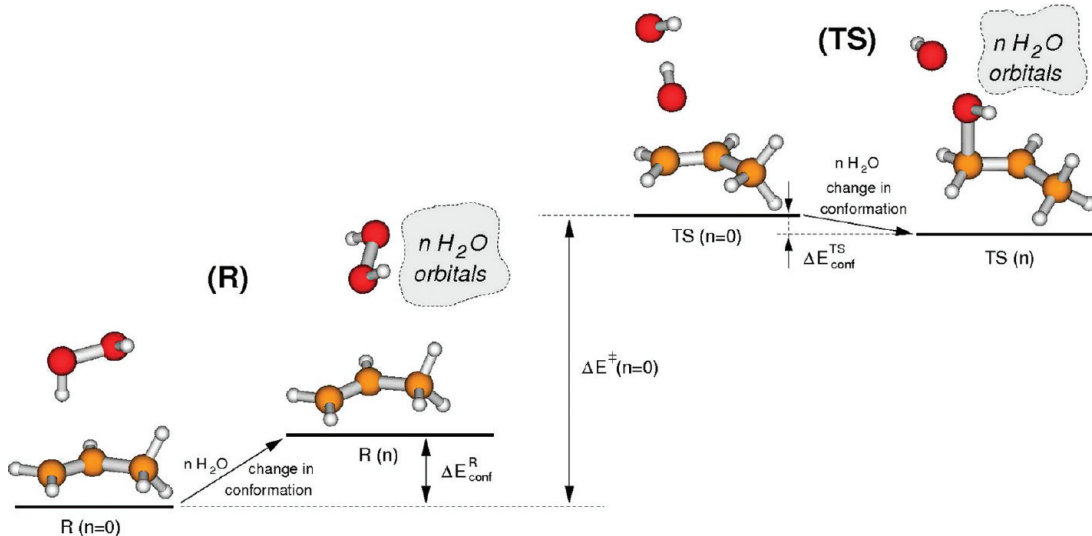


Figure 5. Schematic representation of the propene–H₂O₂ conformational component (ΔE_{conf}) of the reaction barrier.

take up a number of energetically similar conformations around reactants or products. We believe that small differences in calculated reaction energies originate mainly in conformational flexibility of the system and that this effect is relatively unimportant for the problem at hand. We therefore conclude that additional water molecules have no discernible effect on the reaction energy.

These results make it clear that only the addition of the first water molecule has a noticeable effect on the reaction barrier (ΔE^\ddagger). A decrease of about 10 kcal/mol is observed if (any number of) water molecules are present around the propene–H₂O₂ complex. Such a trend is not reflected in geometric parameters and atomic charges of the transition states. Each additional water molecule has the effect of that the TS occurs earlier (i.e., the C(1)O distance noticeably increases) and that the attacking oxygen atom is more equidistant from both double-bonded carbons. As in a concerted process, the dissociation of O–O in H₂O₂ and elongation of the C=C bond is less promoted with increasing n . The O–O and C=C bonds become more polarized with the addition of each successive water molecule, as is reflected in the difference of corresponding atomic charges, but this effect is less pronounced for larger values of n . The imaginary frequency of the transition state exhibits a similar trend. Its magnitude is significantly changed upon addition of the first water molecule but much less so with successive ones.

To clarify the change in ΔE^\ddagger as function of n as opposed to the steady trend in transition state geometry, we analyzed

in detail the contributions to the activation barrier. The model was divided into the propene–H₂O₂ complex, which is common to all systems and represents the uncatalyzed (bare) reference reaction and the cluster of n water molecules. The barrier to epoxidation with n water molecules can then be partitioned, relative to the bare reaction, in the following way: (1) Conformational change in the propene–H₂O₂ subset on interaction with water molecules, both for reactants ($\Delta E_{\text{conf}}^{\text{R}}$) and the transition state ($\Delta E_{\text{conf}}^{\text{TS}}$) (Figure 5). (2) Interaction energy between the subsets, mainly, due to hydrogen bonding, both in reactants ($\Delta E_{\text{HB}}^{\text{R}}$) and in the transition state ($\Delta E_{\text{TB}}^{\text{TS}}$) (Figure 6). (3) Conformational change within the water cluster when passing from reactants to the transition state ($E_{n\text{H}_2\text{O}}^{\text{TS}} - E_{n\text{H}_2\text{O}}^{\text{R}}$) (Figure 7). We note that the components outlined above have all been calculated by using the basis functions of the complete system, along with the corresponding molecular subsets, whereby basis set superposition errors are essentially compensated for. On the basis of the above partitioning scheme the difference between the barrier in presence of n water molecules, $\Delta E^\ddagger(n\text{H}_2\text{O})$, and that of the bare reaction, $\Delta E^\ddagger(n = 0)$, can be expressed as

$$(\Delta E^\ddagger(n\text{H}_2\text{O}) - \Delta E^\ddagger(n = 0)) = (\Delta E_{\text{conf}}^{\text{TS}} - \Delta E_{\text{conf}}^{\text{R}}) + (\Delta E_{\text{HB}}^{\text{TS}} - \Delta E_{\text{HB}}^{\text{R}}) + (\Delta E_{n\text{H}_2\text{O}}^{\text{TS}} - \Delta E_{n\text{H}_2\text{O}}^{\text{R}})$$

The components of reaction barrier as functions of n are listed in Table 3. It is found that the energy of the

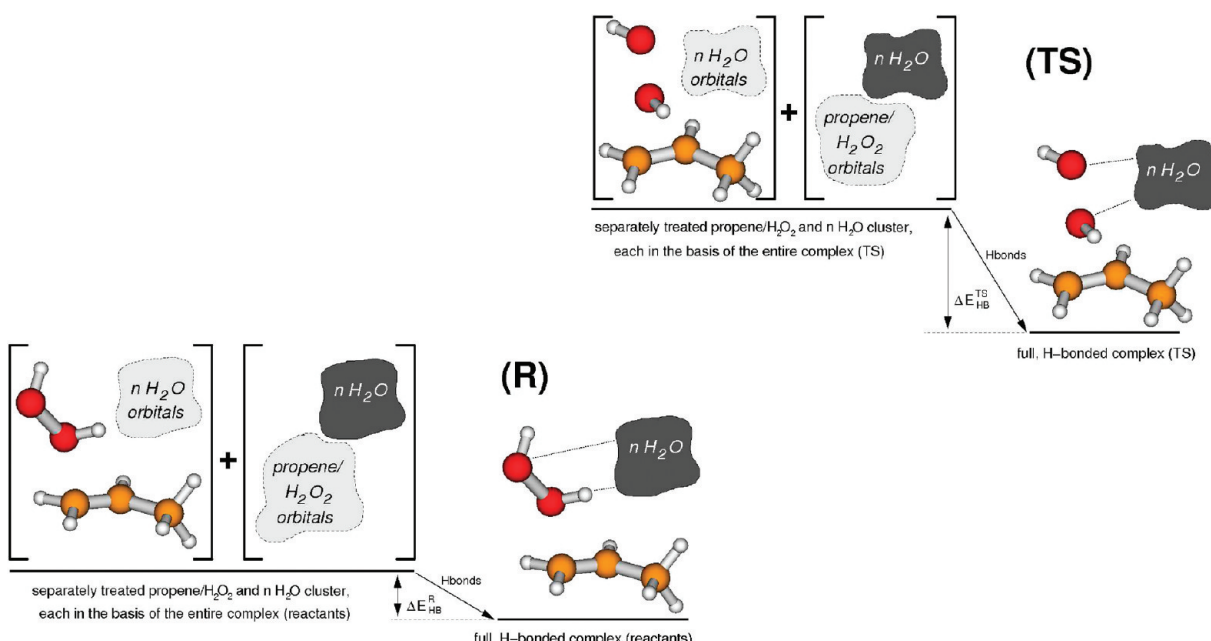


Figure 6. Schematic representation of the stabilization component from the formation of hydrogen bonds (ΔE_{HB}) of the barrier to the reaction.

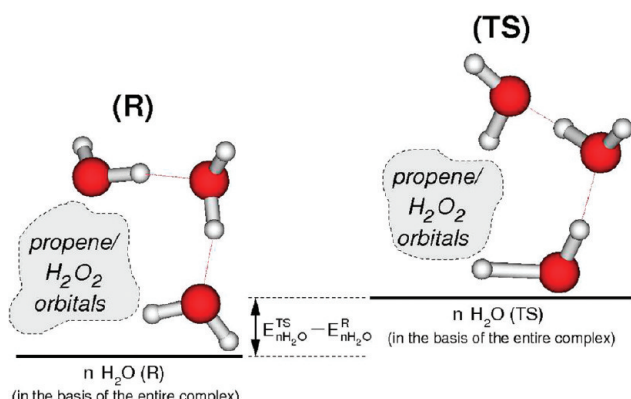


Figure 7. Schematic representation of the water cluster conformational component ($E_{n\text{H}_2\text{O}}^{\text{TS}} - E_{n\text{H}_2\text{O}}^{\text{R}}$) of the reaction barrier.

Table 3. Components of Reaction Barrier for Propene Epoxidation^a

<i>n</i>	$\Delta E_{\text{conf}}^{\text{TS}}$	$\Delta E_{\text{conf}}^{\text{R}}$	$\Delta E_{\text{HB}}^{\text{TS}}$	$\Delta E_{\text{HB}}^{\text{R}}$	$E_{n\text{H}_2\text{O}}^{\text{TS}} - E_{n\text{H}_2\text{O}}^{\text{R}}$	$\Delta E^{\ddagger}(n\text{H}_2\text{O}) - \Delta E^{\ddagger}(n = 0)$
1	0.1	1.9	-14.5	-6.2	0.7	-9.5
2	1.0	2.7	-26.2	-13.7	3.3	-11.0
3	-0.7	0.8	-30.1	-17.8	4.4	-9.4
4	-1.2	3.3	-32.4	-21.0	5.8	-10.2
5	-1.3	-0.1	-33.5	-19.0	5.5	-10.2

^a $\Delta E_{\text{conf}}^{\text{TS}}$ and $\Delta E_{\text{conf}}^{\text{R}}$, energies of conformational change for the propene–H₂O₂ subset on addition of a *n*H₂O cluster for transition states and reactants, respectively; $\Delta E_{\text{HB}}^{\text{TS}}$ and $\Delta E_{\text{HB}}^{\text{R}}$, hydrogen bonding stabilization energies between the subsets, for transition states and reactants; ($E_{n\text{H}_2\text{O}}^{\text{TS}} - E_{n\text{H}_2\text{O}}^{\text{R}}$), change in energy of the *n*H₂O cluster on passing from reactants to the transition state; $\Delta E^{\ddagger}(n\text{H}_2\text{O}) - \Delta E^{\ddagger}(n = 0)$, activation barrier with *n* water molecules relative to the bare reaction with *n* = 0. See text and Figures 5–7 for explanation of the partitioning scheme. All components are given in kcal/mol and are counterpoise corrected for basis set superposition error.

propene–H₂O₂ subset in the transition state does not vary significantly with *n*, even though its structure is affected considerably by the presence of water molecules. This can be explained in terms of a compensation of two opposing

effects. As propene and hydrogen peroxide molecules approach one another in the case with smaller *n* their interaction energy increases, which provides more stabilization. On the other hand the dissociation of H₂O₂ takes up more energy. The propene–H₂O₂ subset of the reactants also does not exhibit a significant energy dependence on *n*, mainly, because of the shallow potential energy surface for positioning of H₂O₂ near propene molecule. In most cases, the addition of water slightly destabilizes the structure of the propene–H₂O₂ subset, most likely because H₂O₂ is slightly pushed away from the propene and its orientation is tilted so that their interaction is weakened. The combination of the conformational changes of reactants and transition states contributes to a small (1.2–1.8 kcal/mol) lowering of the barrier relative to the bare reaction. For *n* = 4, the lowering is more pronounced (4.5 kcal/mol); however, both components are within the same range as for the cases *n* = 1, 2, 3 or 5. The differences are therefore likely to be the result of the extensive conformational flexibility of the system.

Both reactants and transition states are stabilized to a significant extent by the formation of hydrogen bonds. Because of the synergistic effect of multiple hydrogen bonds, stabilization increases with *n*, but each added water molecule brings less of a gain in stabilization energy. Not surprisingly, this stabilization effect is much more pronounced for the transition states than for the reactants because the H₂O₂ molecule is more polarized in the former and thus capable of establishing stronger hydrogen bonds with water. The difference in stabilization energy between the transition state and reactants is -8.3 kcal/mol for *n* = 1 and about -12 kcal/mol for *n* = 2. Beyond that each additional water molecule provides roughly the same degree of stabilization for both reactants and the transition state, so that ($\Delta E_{\text{HB}}^{\text{TS}} - \Delta E_{\text{HB}}^{\text{R}}$) does not increase in magnitude and remains at about -12 kcal/mol for *n* ≥ 2.

The increase in hydrogen bond interactions when passing from reactants to the transition state is also accompanied by

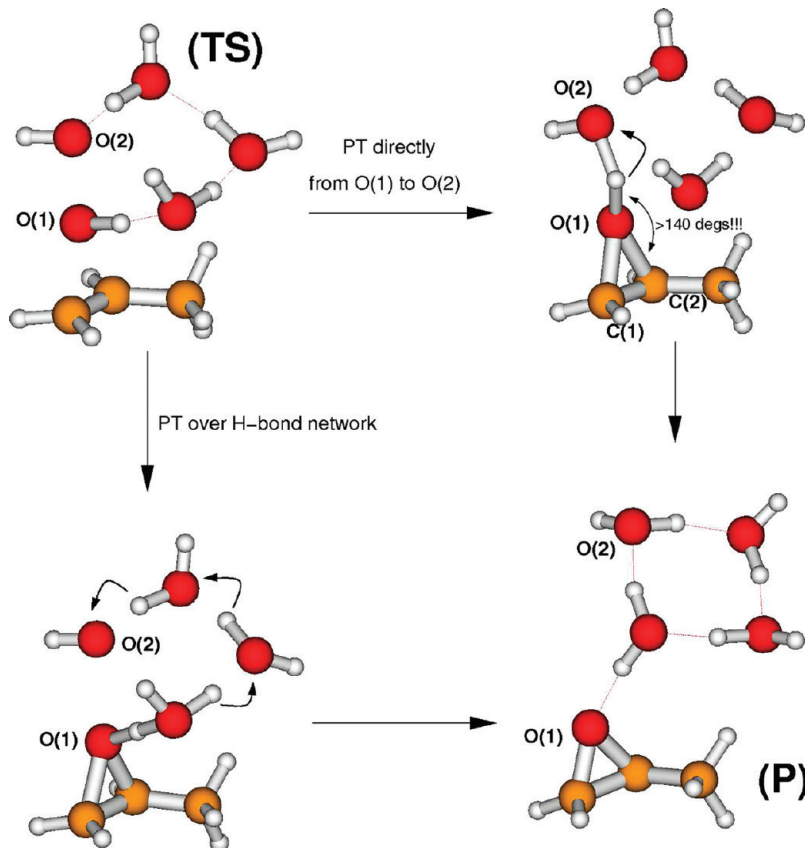


Figure 8. Two alternative mechanisms of proton transfer (PT) from O(1) to O(2) in the process of conversion of the transition state (TS) to products (P).

structural changes within the water clusters. Perhaps the most significant change is the elongation of the O–H distance in the water molecule which acts as the proton donor in the hydrogen bond with hydrogen peroxide. Such an elongation requires energy and thereby reduces the stability of the water cluster. This effect, however, is balanced by energy stabilization upon formation of the hydrogen bond, but the latter effect is not accounted for in the water cluster itself. The energy increase for $n\text{H}_2\text{O}$ is larger when this cluster establishes stronger hydrogen bonds with the propene– H_2O_2 subset. As is the case with hydrogen-bond derived stabilization, the change in ($E_{n\text{H}_2\text{O}}^{\text{TS}} - E_{n\text{H}_2\text{O}}^{\text{R}}$) is only pronounced when passing from $n = 1$ to $n = 2$, but is essentially unchanged for $n \geq 2$. When the three terms of the transition energy partitioning scheme are combined, we may conclude that conformational changes in the propene– H_2O_2 subset are mostly independent of n , while trends in the two other terms distinguish between $n = 1$ and $n > 1$, with the one-step changes in these terms (when passing from $n = 1$ to $n = 2$) having nearly equal magnitudes but opposite signs. Therefore, the effects which contribute to the lowering of the reaction barrier when n additional water molecules are added (relative to $n = 0$) cancel out, whereby we obtain virtually the same catalytic activity of n water molecules, that is, a barrier lowered by 10 kcal/mol, for any number $n \geq 1$ of water molecules.

We have attempted to determine the reaction profile with the use of the intrinsic reaction coordinate (IRC) approach, as implemented in the *Gaussian 03* program package. De Visser et al.¹⁶ previously reported that the epoxidation mechanism is a concerted process, which includes the transfer of the excess proton originally bonded to O(1) back to O(2)

to form a water molecule. In the case of the reaction without water molecules ($n = 0$), the proton is transferred directly from O(1) to O(2), as suggested by the atomic motions involved in the imaginary vibrational mode. Surprisingly, IRC predicts the same kind of a mechanism (direct proton transfer from O(1) to O(2)) even in the presence of water molecules in the vicinity of the reacting species. Both mechanisms of proton transfer are illustrated in Figure 8 for $n = 3$. Despite the fact that the water molecules are arranged in a circular hydrogen-bonded network, which links both parts of the dissociating H_2O_2 molecule, the proton transfer from O(1) to O(2) predicted by IRC does not make use of this virtually strainless pathway by means of a series of short hydrogen bonds but rather has the proton migrate directly from O(1) to O(2) in a process that involves the highly unfavorable breaking of an O(1)–H \cdots O hydrogen bond along with the deformation of the C(1)–O(1)–H and C(2)–O(1)–H angles up to values of 147°. There are a number of reasons why we believe that the IRC prediction of the latter mechanism not to be reliable. IRC pathways are based on vibrational modes calculated in the harmonic approximation, whereas it is well known that modes involving short hydrogen bonds exhibit a large degree of anharmonicity. The double-well nature of the proton potential in the O–H \cdots O hydrogen bonds in particular, which is established in the transition state, is not accounted for by the IRC, so that a concerted multiple proton transfer mechanism is ruled out without adequate physical basis. We have also performed an NBO analysis of the stabilizing interactions of the lone pairs on oxygen atoms with the O–H antibonding orbitals, which may be viewed as a measure of the affinity of that particular lone pair and the proton. Some

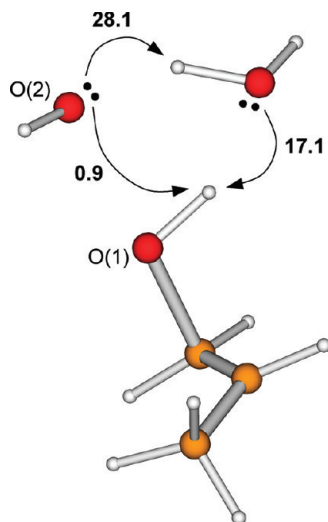


Figure 9. Selected NBO donor–acceptor stabilization energies of lone pair electrons on oxygen atoms and vacant O–H antibond orbitals (in kcal/mol) for the gas-phase propene epoxidation transition state with one additional water molecule ($n = 1$).

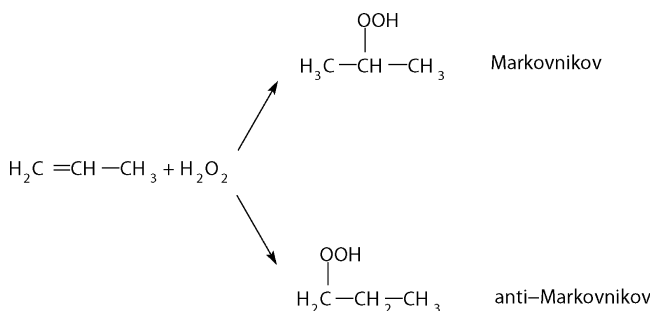


Figure 10. Addition of hydrogen peroxide to propene: Markovnikov and anti-Markovnikov type.

significant interaction energies in the transition state and with $n = 1$ are shown on Figure 9. The interaction of the lone pair on O(2) with the migrating hydrogen (the one assumed to be predominant by IRC) is only 0.9 kcal/mol, whereas analogous interactions for established hydrogen bonds are much stronger, namely, 17.1 and 28.1 kcal/mol in the present case. It is therefore much more reasonable to believe that the proton transfer from O(1) to O(2), which is an essential part of the transformation of the transition state to products, utilizes the network of hydrogen bonds formed by surrounding water molecules rather than the direct transfer not mediated by water molecules.

3.2. Gas-Phase Model: An Alternative Mechanism. A reasonable alternative reaction pathway for the propene– H_2O_2 system is the polar addition of H_2O_2 to the C=C double bond, which would lead either to the formation of 2-hydroperoxopropane (Markovnikov) or 1-hydroperoxopropane (anti-Markovnikov) (Figure 10). As shown in section 3.1 and in ref 16, the epoxidation of propene in the gas phase is a concerted process involving the formation of the epoxide simultaneously with dissociation of H_2O_2 and formation of a water molecule. We believe that under the same conditions the addition of H_2O_2 to the C=C double bond will also undergo a concerted polar mechanism including simultaneous dissociation of H_2O_2 to H^+ and OOH^- and their addition to the double bond. On the other hand, we consider a radical and purely ionic mechanism to be much less likely because of high activation energies as the calculated dissociation

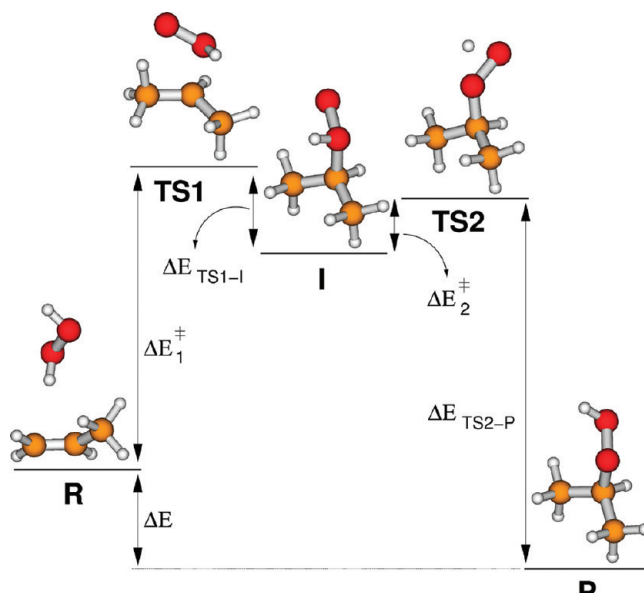


Figure 11. Mechanism of the Markovnikov-type addition of H_2O_2 to propene. Structure labels: R, reactants; TS1, first transition state; I, reactive intermediate; TS2, second transition state; P, products. Note that the structures correspond to the Markovnikov-type reaction; the corresponding anti-Markovnikov structures are analogous, with the OOH group being shifted from the middle carbon atom to the lateral one.

energy of H_2O_2 in the gas phase is 380.5 kcal/mol. Moreover, the addition of the OOH^- anion to propene does not yield any stable structure that could possibly allow for the incorporation of H^+ to complete the reaction. The adduct either releases OH^- and thereby yields propene oxide, or the OOH^- anion simply dissociates from propene and leaves it effectively intact. We therefore studied the concerted polar addition mechanism in the presence of zero, one, and two spectator water molecules ($n = 0, 1$, and 2).

We found that the concerted polar addition of H_2O_2 to propene is essentially a two-step reaction in contrast to the epoxidation reaction. It is schematically displayed on Figure 11. In the first step a reactive intermediate is formed with H^+ and OOH^- bonded to either side of the original C=C bond. The hydroperoxy group is, however, connected to carbon by way of the O(H) terminal rather than the other oxygen atom. The latter has an unsaturated valence and would normally be assumed to be available for bonding, but the OOH group bonded in this way may be regarded as dipolar. Despite the fact that such a structure has an unusual appearance, it was shown to correspond to a true minimum on the potential energy surface by frequency calculations. The first step is subject to a barrier of about 30 kcal/mol, depending on whether the mechanism is of a Markovnikov or anti-Markovnikov type and on the number of spectator water molecules, as discussed below. The reaction intermediate then undergoes a proton transfer from the oxygen, which is directly bonded to carbon, back to the more remote oxygen with the extra valence by passing over a transition state with a much lower barrier. It was found to be 10 kcal/mol in the most extreme case, but typically low enough to suggest a nearly barrierless transition of the intermediate to products.

The energies of distinct steps of the reaction are listed in Table 4. The rate determining step in the addition reaction is the approach of H_2O_2 molecule to propene; the second

Table 4. Energy Parameters (in kcal/mol) of the Addition Reaction of H₂O₂ to Propene^a

<i>n</i>	type	ΔE	ΔE_1^\ddagger	ΔE_2^\ddagger	$\Delta E_{TS1 \rightarrow I}$	$\Delta E_{TS2 \rightarrow P}$
0	M	-17.1	34.8	9.2	-11.0	-50.7
0	AM	-14.2	40.5	8.8	-12.4	-51.1
1	M	-17.0	30.5	1.8	-16.1	-33.2
1	AM	-14.0	34.9	1.6	-17.4	-33.1
2	M	-17.0	28.7	0.8	-18.9	-27.5
2	AM	-13.7	33.7	1.4	-19.7	-29.1

^a See Figure 11 for the explanation of terms. *n* corresponds to number of additional water molecules, and the reaction type labels are the following: M, Markovnikov; AM, anti-Markovnikov.

step involving hydrogen transfer from the attacking oxygen to the lateral one requires much less energy. Therefore ΔE^\ddagger is the legitimate measure for the activation and for the reaction kinetics. Additional water molecules further diminish ΔE_2^\ddagger and nearly reduce the reaction to a single step. It is evident that the Markovnikov type is preferred both in terms of reaction energy and barrier: the Markovnikov mechanism is about 3 kcal/mol more exothermic than anti-Markovnikov and the barrier about 5 kcal/mol lower. We found that additional water molecules do not have an impact on reaction energy, but do slightly lower the barrier from 34.8 kcal/mol for *n* = 0 to 28.7 kcal/mol for *n* = 2.

A comparison of this reaction with the epoxidation mechanism reveals that there is little, if any difference in the reaction barrier for *n* = 0. When one or two water molecules are introduced the barrier to epoxidation is lower than the one for the addition reaction by 4.8 and 4.5 kcal/mol, respectively. The reaction energy for the addition, on the other hand, is about three times or 35 kcal/mol less exothermic than that for epoxidation. The epoxidation pathway is therefore significantly thermodynamically preferred over that for addition. Since the addition reaction does not in any case exhibit low barriers either, we conclude that it cannot compete with epoxidation.

3.3. Influence of Solvation. It is a reasonable assumption that much of the activity of the real catalyst can be attributed to the fact that the complex framework, including the channels surrounded by polar Si—O bonds and titanium-doped active sites, provides an effective polar environment that enhances its catalytic activity. We therefore investigated the influence of the polar environment on the reaction profile. Structures of reactants, products, and transition states for the propene epoxidation reaction were optimized in the same manner as with the gas phase model in this case with the use of the IEFPCM solvation method. A dielectric constant of 78.4, which corresponds to that of water, was used to model the solvent. Reactions involving only propene and hydrogen peroxide, as well as one or two added water molecules (*n* = 0, 1, and 2), were considered. We note that we encountered several difficulties with calculations based on the IEFPCM solvation model. In particular, geometry optimizations converged poorly and often required hundreds of steps to complete; structures of the products for *n* = 2 did not converge even after 300 geometry steps and a number of restarts. In addition, in a few cases, the calculated harmonic frequencies were not all positive; imaginary frequencies were found particularly for transition state structures. For *n* = 1 and 2, we observed one redundant imaginary mode at 67 *i* cm⁻¹; the mode mainly consists of

torsional motion of the water molecule relative to propene and HO···OH moieties. Because of its small magnitude, we considered this error relatively unimportant. For *n* = 0 however, the redundant imaginary mode was calculated to 214 *i* cm⁻¹, and the mode involves coupled torsional and stretching motion of the remote OH group. The difference in the description of the redundant imaginary mode provides additional evidence that the reaction mechanism in the absence of water molecules is notably different from the situation where additional water molecules provide an alternative proton transfer pathway.

The main characteristics of the reaction and of the transition state are shown in Table 5. The most notable difference to the gas-phase model is the significant lowering of the barrier to the reaction. While reaction energies remained virtually the same when the continuum solvent is included (about -55 kcal/mol), the barrier is lowered by 10 kcal/mol even for the model without water molecules (*n* = 0). Introduction of one water molecule results in a substantial lowering of the barrier (by 8.5 kcal/mol) in a similar manner as in the gas phase model. The addition of a second water molecule, on the other hand, did not lower the barrier any further, and instead resulted in an increase by 2.7 kcal/mol to a value of 19.6 kcal/mol. A comparison with the corresponding gas-phase transition states for *n* = 0, 1, and 2 (Table 2) reveals that in the solvent continuum model, the transition state occurs earlier by all geometric criteria. The natural atomic charge on O(2) in the continuum model is slightly more negative than in the gas phase and tends to become less negative with increasing *n* unlike the trend in the gas phase. The lowering of the barrier as result of solvation can be explained by the fact that polar solvent provides an excess in the stabilization energy of the transition state relative to the gas phase. The transition state is highly polarized unlike the reactants and products because of the large O···O separation caused by breaking up the hydrogen peroxide molecule. This is supported by the fact that the dipole moment of reactants or products is of the order of 1–2 D, while for the transition state, it is notably higher, namely, about 5 D.

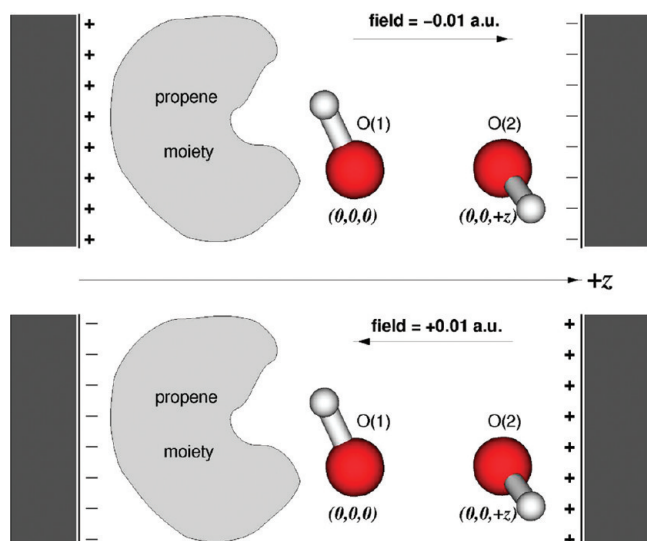
Because the effective dielectric constant inside the zeolite channel is likely to be smaller than that of bulk water, we have also calculated the reaction energy and barrier for a tentative value of ϵ = 5 (*n* = 0, 1 and 2), which is a more reasonable estimate for an environment inside the zeolite. As was the case with the more polar solvent model, the reaction energy remains virtually unaltered, but the barrier was found to be reduced by about half as much as with water as solvent, being about 29 kcal/mol for *n* = 0 and just over 20 kcal/mol for *n* = 1 and 2. The effect of lowering the barrier with respect to the gas phase is still significant, even with the smaller dielectric constant.

3.4. Influence of Electric Field. Calculations which include the presence of an electric field may be viewed in a similar vein as those with the solvent reaction field, except for the important difference that the externally applied electric field has an adjustable direction. We chose the direction of the field to be aligned along the O(1)···O(2) line. We believe that such a model can mimic some of the electrostatic interactions imposed by the titanium active site of a titanasilicalite zeolite-type catalyst, which in turn could be crucial for understanding its catalytic activity.

Table 5. Propene Epoxidation Reaction Treated with the Polarizable Continuum Solvation Method of Tomasi at the B3LYP/6-31+G(d,p) Level of Theory and Water ($\epsilon = 78.4$) As Solvent^a

<i>n</i>	ΔE	ΔE^\ddagger	$R_{C(1)O}$	$R_{C(2)O}$	R_{OO}	R_{CC}	ν^\ddagger	natural charge			
								O(1)	O(2)	C(1)	C(2)
0	-55.6	25.4	1.903	2.221	1.974	1.383	517	-0.602	-0.921	-0.317	-0.051
1	-58.7	16.9	1.933	2.192	1.923	1.379	505	-0.589	-0.908	-0.323	-0.075
2	-55.0 ^c	19.6	2.003	2.189	1.889	1.375	502	-0.586	-0.881	-0.333	-0.069

^a Reaction energy (ΔE) and barrier (ΔE^\ddagger) (both in kcal/mol), selected metric parameters of the transition state (in Å), the imaginary transition state harmonic frequency (ν^\ddagger , in $i\text{ cm}^{-1}$), and natural charges of selected atoms, calculated with different number of explicit water molecules (*n*) in the model. See Figure 2 for explanation. ^b Two imaginary frequencies; the one not displayed assumed a value of $214 i\text{ cm}^{-1}$ for *n* = 0 and $67 i\text{ cm}^{-1}$ for *n* = 1 and 2. ^c Geometry optimization of products not converged after 300 cycles.

**Figure 12.** About the modeling of external electric field.

It is generally thought that the presence of a particular electrostatic field inside the pore of a zeolite has an appreciable effect on the function of these materials as catalysts. To explore this effect, calculations were performed to assess the dependence of reaction free energies and activation barriers on an applied external electric field. The purpose of these calculations is to determine the value of an applied electric field across the system that would lead to significant changes in thermodynamic parameters. It must be stressed that the values used for the electric field are thereby somewhat arbitrary, although they are similar in magnitude to fields applied experimentally in preliminary studies of the effect of electric fields on adsorption properties.³⁷

The application of an external dipolar field can be viewed as being equivalent to placing the system between two parallel, oppositely charged plates of a capacitor in such a way that the plates are always perpendicular to the O(1)…O(2) line, as shown in Figure 12. The resulting field is parallel to the O(1)…O(2) line. A constant field of 0.01 atomic units was applied in either direction, that is, which could have either a positive or negative sign.

Table 6 shows the reaction energetics, selected geometry details and the atomic charges of the transition state for *n* = 0 and *n* = 1 as function of external dipolar electric field applied parallel to the O(1)…O(2) axis (see Figure 2), and a comparison with the analogous results without external field. The negative field gives rise to an appreciable increase in the reaction barrier of about 12 kcal/mol and a later occurrence of the transition state, which is reflected mainly

in the shortening of $R_{C(1)O}$. The barrier, on the other hand, is significantly reduced when the field changes sign, by as much as 14.5 (*n* = 0) or 9.8 kcal/mol (*n* = 1), and the transition state occurs earlier, as reflected by the considerable increase of the C(1)…O(1) distance. As expected, the polarity of the O…O and C=C bonds is increased when the field is switched from negative to positive. The imaginary frequencies of transition state, however, do not exhibit any trend with the electric field.

The effect of the application of an external electric field on the reaction energy appears to differ markedly from that of adding several water molecules or of the solvent reaction field, in that a positive field make the reaction energy more negative, whereas a negative field makes it less negative, at least for *n* = 1. This observation suggests that the influence of the electric field may go beyond being catalytic in nature in the sense that it does affect ΔE . We therefore analyzed the impact of the field on the basic electrostatic properties of the species involved in the course of the reaction to clarify these results. We performed single-point calculations on gas-phase optimized reactants, transition state, and products in an applied electric field of both signs to study changes in electrostatic properties. Results are summarized in Table 7.

The *z* component of the dipole moment, μ_z , for all species tends to become more positive under the negative field and more negative under the positive field. The magnitude of this change is proportional to the isotropic *z* component of polarizability, α_{zz} . Thus the sensitivity of μ_z toward the external field is much larger in the transition state than in the reactants or products which confirms the observed sensitivity of ΔE^\ddagger to the electric field. The *z* component of the dipole moment of the reactants is lowest for all the species, and it changes sign upon application of a positive field. As the interaction energy between the dipole and the electric field is proportional to the product of their values, reactants appear to be stabilized under both a negative or positive field. Such a trend is not observed for the products, because the *z* component of their dipole moment takes on larger absolute values and does not change sign with the field. The energy of the products exhibits a different trend as a function of the external field, which explains the significant change in ΔE as a result of the interaction with the field. A limitation of this model of the external applied electric field parallel to the O(1)…O(2) axis lies in the fact that this orientation is less appropriate for the products than for the reactants or the transition state. While in the latter case, the two O(1) and O(2) atoms form a well defined peroxide moiety, its nature is completely lost in the products. Although many aspects of this type of simplified model for

Table 6. Reaction Energies (ΔE) and Barriers (ΔE^\ddagger) of the Propene Epoxidation Reaction and Selected Atomic Distances (see Figure 2; in Å), Imaginary Frequencies (ν^\ddagger , in $i\text{ cm}^{-1}$), and Natural Atomic Charges of the Transition State for the Propene Epoxidation Reaction in the Presence of External Electric Field along the O(1)…O(2) Line^a

n	field	ΔE	ΔE^\ddagger	$R_{C(1)O}$	$R_{C(2)O}$	R_{OO}	R_{CC}	ν^\ddagger	natural charge			
									O(1)	O(2)	C(1)	C(2)
0	—	-56.4	47.3	1.554	2.229	1.952	1.428	465	-0.569	-0.721	-0.229	-0.246
	0	-52.6	35.2	1.677	2.235	1.979	1.403	509	-0.599	-0.823	-0.276	-0.115
	+	-61.1	20.7	1.830	2.332	1.955	1.388	432	-0.602	-0.870	-0.313	-0.052
	—	-51.6	38.4	1.591	2.225	1.899	1.418	348	-0.556	-0.748	-0.237	-0.250
1	0	-57.0	25.7	1.757	2.191	1.949	1.392	448	-0.581	-0.850	-0.290	-0.100
	+	-62.7	15.9	1.935	2.374	1.891	1.379	388	-0.577	-0.848	-0.330	-0.058

^a The field is labeled as follows: 0, no field; —, field of -0.01 a.u.; +, field of +0.01 a.u. Note that the positive direction along O(1)…O(2) is defined as a vector that starts on O(1) and ends on O(2). For a more detailed explanation, see text.

Table 7. Component of Dipole Moment Parallel to External Electric Field ($\mu_z D$) at Various Magnitudes of the Field, Isotropic Component of the Polarizability Tensor along z at Zero Field (α_{zz} , in bohr³), and the Energy Change on Interaction with the External Field Relative to Field = 0 (ΔE_F , in kcal/mol) for Reactants (R), Products (P), and Transition State (TS) of the Propene Epoxidation Reaction ($n = 0$) Calculated As Single Points at the B3LYP/6-31+G(d,p) Level of Theory^a

species/field	μ_z			α_{zz}			ΔE_F		
	—	0	+	0	—	0	+	—	0
R	2.15	0.53	-1.08	63.5	-3.3	0.0	-0.7		
P	-1.07	-2.32	-3.57	49.0	+4.2	0.0	-7.3		
TS	-1.79	-5.48	-9.21	145.4	+9.0	0.0	-18.1		

^a Optimized structures of R, P, and TS in the gas phase have been used. Field labels: —, -0.01 a.u.; 0, no field; +, +0.01 a.u.

Table 8. Propene Epoxidation Reaction Energy (ΔE) and Barrier (ΔE^\ddagger) (both in kcal/mol), Selected Metric Parameters of the Transition State (in Å), and the Imaginary Transition State Harmonic Frequency (ν^\ddagger , in $i\text{ cm}^{-1}$), Calculated with the Cluster Representation (11T) of the TS-1 Zeolite Catalyst and in Presence of Different Number of Water Molecules (n)^a

n	ΔE	ΔE^\ddagger	$R_{C(1)O}$	$R_{C(2)O}$	R_{OO}	R_{CC}	ν^\ddagger
0	-55.5	25.8	1.840	2.113	1.918	1.385	453
1	-55.5	22.0	1.949	2.076	1.886	1.379	488
2	-56.2	24.9	1.896	2.320	1.892	1.376	481

^a See Figures 2 and 4 for explanation.

catalytic activity are likely to be somewhat inadequate, the influence of electrostatic interactions on the reaction barrier is undoubtedly of significance, and leads us to conclude that it should play a critical role in activity of the titanosilicalite catalysts.

3.5. QM and QM/MM Cluster Models. The optimized geometries and energies of reactants, products, and transition states for propene epoxidation at the reaction center embedded in a zeolite cluster model were obtained in a similar way as described in sections 2 and 3.1. Zero, one, or two spectator water molecules were used with this model. Table 8 lists the reaction and activation energies and characteristics of the transition state. The calculated reaction energy was found to vary only marginally with n and to be in the same range as calculated with gas-phase, solvent, and external field models. In contrast to the result for the gas phase model, the calculated barrier does not decrease significantly upon the addition of the first water molecule and remains instead at about 25 kcal/mol or somewhat below that. The addition of this water molecule causes the barrier to decrease to 22

kcal/mol. We do not believe this change to be significant, however, because of the conformational freedom of the system discussed above. Indeed, the barrier rises again to nearly 25 kcal/mol when the second water molecule is added. From the point of view of geometry, the transition state occurs notably earlier than in the uncatalyzed reaction, and there is no significant difference for $n = 0, 1$, and 2. The fact that for $n = 1$, the transition state occurs slightly earlier than in the other two cases, however, correlates well with the lower barrier observed for $n = 1$.

The zeolite-type environment represented by the cluster does indeed lower the barrier with respect to the uncatalyzed reaction, but its effect is rather weak, namely, of similar magnitude as the addition of a single water molecule in the gas phase calculation. The effect of the zeolite environment on the occurrence of the transition state is similar to that of three water molecules. Our computed catalytic activity is rather modest, which suggests that either the zeolite model used in our study lacks essential size and flexibility or otherwise poorly describes some of the crucial features of the zeolite active site, or that the actual reaction mechanism in the zeolite channel differs in a significant way from the one we assumed. Previous studies¹³ have suggested that the catalytic activity of TS-1 could originate from a hydrolysis of one the Ti–O–Si bonds. Because the hydrolyzed Si(OH) and particularly the five-ligand coordinated Ti(OH) groups may well be more reactive than the unhydrolyzed zeolite framework, we also modeled the propene epoxidation reaction using a hydrolyzed 11T cluster. Our initial studies of the hydrolysis of the cluster suggested that one site was thermodynamically preferred. We therefore looked into the essential stages of propene epoxidation in the presence of this hydrolyzed cluster model. The resulting transition state geometry is shown on Figure 13.

Note that the hydrolyzed zeolite cluster model considered in this study does not contain added water molecules. For hydrolysis to occur, however, the addition of one water molecule is essential, so that we may regard this model to implicitly contain one water molecule. The calculated reaction energy (ΔE) and barrier (ΔE^\ddagger) of -50.7 and 23.5 kcal/mol, respectively, are in the same range as for the unhydrolyzed model. The hydrolyzed model of TS-1 therefore does not yield a significant improvement in the catalytic activity.

It is important to note that the limitation of a finite cluster size is likely to impair the reliability of this type of model. We therefore attempted to create a more realistic description

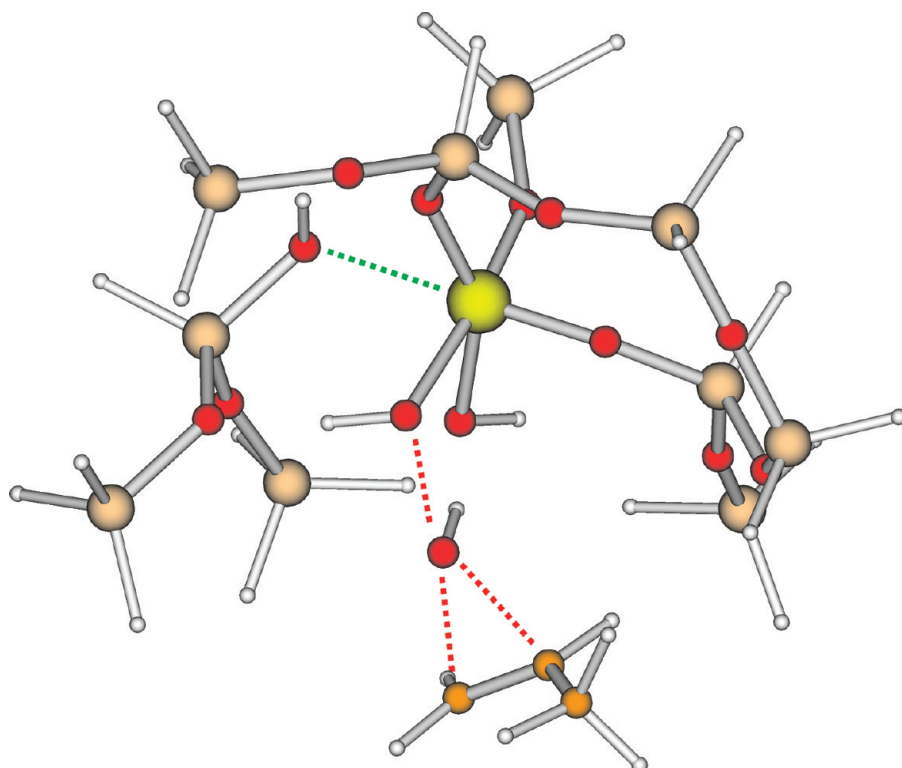


Figure 13. Propene epoxidation transition state in the presence of the 11T hydrolyzed cluster representing the TS-1 active site. Green dashed line denotes the hydrolyzed Ti–O–Si link, and the red dashed lines correspond to the dissociating O···O bond and the forming C–O epoxide bonds.

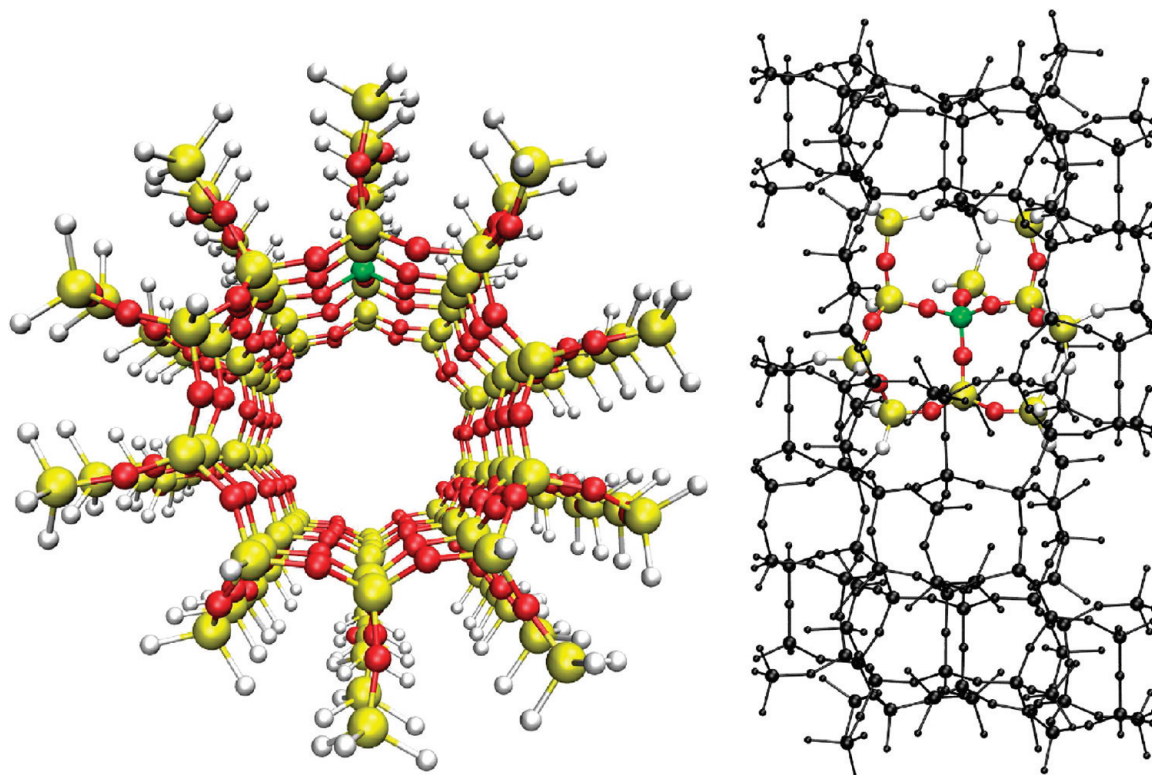


Figure 14. QM/MM ONIOM model of the main channel of TS-1. Left: Top view. Right: Side view. QM atoms shown as color balls and sticks and MM atoms represented as black, thinner balls and sticks. Atom coloring: white, hydrogen; red, oxygen; yellow, silicon; green, titanium.

of the zeolite environment by construction of an embedded two-layer QM/MM system. The 11T QM (B3LYP) cluster defined above was inserted into a larger cylindrical representation of the zeolite pore (Figure 14), consisting of a total

number of 436 atoms (120 Ti/SiO₄ tetrahedra, a “120T cluster”). This embedding methodology is implemented in the *Gaussian 03* software using the ONIOM protocol.³⁸ The molecular mechanics interactions were treated using the

universal force field (UFF) as developed by Rappé and co-workers.³⁹ The same 6–31G(d,p) basis set was used for the sorbate molecules for the QM cluster. However, despite our best efforts, the QM/MM methodology yielded rather disappointing results. First of all, no meaningful geometry optimization was possible when the charge embedding feature (MM charges interacting with the QM wavefunction) was enabled. While the propene epoxidation energy of about 50 kcal/mol could be adequately reproduced even by using a simplified QM/MM methodology without charge embedding, the calculated reaction barriers were found to be highly overestimated, that is, in the range of 43–48 kcal/mol. When only the DFT component of the total ONIOM energy was considered, more plausible results were obtained, which in fact agreed well with those obtained by using the isolated QM cluster. The QM/MM zeolite model used by us also does not favor hydrolysis of the Ti–O–Si or Si–O–Si bonds, a significant drawback in view of important role of the Si–OH and Ti–OH groups outlined by many authors.^{13,29,40,41} Since our QM/MM calculations were mostly of a preliminary nature, the origin of the observed discrepancies are not clear. At this point there are very few published studies available which deal with these aspects in zeolite-type systems. One of the recent ONIOM study of zeolites did not use charge embedding either,²⁸ while an alternative approach of polarizing the QM part of an ONIOM system by using a mesh of point charges yielded plausible results.⁴² A rather more detailed investigation of several factors related to the ONIOM modeling would indeed be highly desirable, while the utilization of a large-scale model of the zeolite pore remains a challenge for the modeling of the catalytic activity of TS-1.

The variety of catalytic mechanisms proposed for the epoxidation of propene in the TS-1 framework deserves to be investigated in greater depth by detailed comparison of a number of reaction pathways. A thorough study of five different mechanisms, based on a comparable cluster DFT methodology, has indeed been recently published,²⁹ whereas the main focus of our work was directed at the assessment of physical factors which influence the epoxidation of propene by hydrogen peroxide. While addressing many other mechanisms for this reaction is therefore beyond the scope of this paper, our results still merit comparison with the findings of Wells and co-workers. Among the five mechanisms they considered, our work coincides with the one proposed by Vayssilov and van Santen.⁴³ While the approach of Wells and co-workers gave a reaction energy barrier of about 19 kcal/mol, which decreased by only 2 kcal/mol relative to the uncatalyzed gas-phase reaction, our calculations show a noticeably larger improvement for the catalyzed reaction, in that the barrier was lowered by about 10 kcal/mol (from 35.2 to 25.8 kcal/mol, when no spectator water molecules are included in either model). These differences between the computed barriers are quite significant. While the differences between the present approach and that of Wells may be attributed in part to model chemistry (different DFT, use of pseudopotentials, different basis set) and to some extent to the different size of the cluster and different structural constraints, they must still be considered as unusually large. Caution in the modeling of this and similar reactive systems is therefore clearly advised. A more detailed examination of factors which have a potential impact on the

activation barrier is needed, but beyond the scope of the present work.

4. CONCLUSIONS

We have successfully applied ab initio quantum chemical techniques to the study of the epoxidation reaction of propene and hydrogen peroxide, both in the gas phase and in the presence of the TS-1 catalyst. For the gas phase process, we find that the reaction occurs by a concerted process involving a proton transfer between the two peroxide oxygens. This process can be effectively mediated by the introduction of water molecules to the model, which serve to facilitate the proton transfer process by hydrogen bond stabilization. We find that one water molecule reduces the barrier by around 10 kcal/mol, the addition of more molecules to the system does not result in a further reduction of the barrier. An analysis of the contributions involved in the computed activation energy suggests that this is the result of a cancelation of two terms in the energy expression. Calculations on the competing, nonconcerted polar addition of hydrogen peroxide to the double bond reveal it to be noncompetitive from a thermodynamic standpoint. Inclusion of a background solvent field to the calculation appears to further reduce the activation energy of the reaction as does the application of a directed electric field along the O–O bond. In both cases, the higher polarizability of the transition state provides the rationalization. Our calculations using models of the TS-1 catalyst provide an interesting comparison with the gas phase results. We find that the presence of the catalyst indeed reduces the activation energy compared to the uncatalyzed reaction in the gas phase, but this reduction is rather weak, and just comparable to that of adding a single water molecule without the catalyst. Many authors have suggested that this reaction mechanism in the zeolite in fact occurs via a different mechanism from that in the gas phase process by involving hydrolysis of the titanium center. Our calculations, however, on models for this pathway show no significant enhancement in the activation energy. This may be the result of the finite size and lack of flexibility in our cluster which is limited by the computational cost of the calculations. The size limitation of the cluster models calls for application of large-scale methodologies such as QM/MM. We were, however, not able to properly assess several important aspects of this type of modeling at the entry level. The utilization of large-scale, size-consistent computational methodology thus remains a critical challenge for the future theoretical work on the catalytic activity of TS-1.

ACKNOWLEDGMENT

J.S. thanks the Center for Non Linear Studies, Los Alamos Neutron Scattering Center, and the LANL LDRD program for a postdoctoral fellowship and the Slovenian Research Agency for financial support (Contract 1000-07-219779). The authors thank Bob Ecke, Richard Martin, Jeff Hay, and Antonio Redondo for useful discussion. Los Alamos National Laboratory is operated by Los Alamos National Security, LLC for the National Nuclear Security Administration of the U.S. Department of Energy under contract DE-AC52-06NA25396. This paper has been designated LA-UR 08-0941.

REFERENCES AND NOTES

- (1) Taramasso, M.; Perego, G.; Notari, B. U.S. Patent 4410501, 1983.
- (2) Notari, B. Microporous crystalline titanium silicates. *Adv. Catal.* **1996**, *41*, 253.
- (3) Hijar, C. A.; Jacobinas, R. M.; Henson, N. J.; Hay, P. J.; Ott, K. C. The siting of Ti in TS-1 is non-random. Powder neutron diffraction studies and theoretical calculations of TS-1 and FeS-1. *J. Phys. Chem. B* **2001**, *104*, 12157–12164.
- (4) Bordiga, S.; Zecchina, A.; Artioli, G.; Marra, G.; Spanò, G. Ti location in the MFI framework of Ti-silicalite-1: A neutron powder diffraction study. *J. Am. Chem. Soc.* **2001**, *123*, 2204–2212.
- (5) Henry, P. F.; Weller, M. T.; Wilson, C. C. Structural investigation of TS-1: Determination of the true nonrandom titanium framework substitution and silicon vacancy distribution from powder neutron diffraction studies using isotopes. *J. Phys. Chem. B* **2001**, *105*, 7452–7458.
- (6) Deka, R. C.; Nasluzov, V. A.; Shor, E. A. I.; Shor, A. M.; Vayssilov, G. N.; Rösch, N. Comparison of all sites for Ti substitution in zeolite TS-1 by an accurate embedded-cluster method. *J. Phys. Chem. B* **2005**, *109*, 24304–24310.
- (7) Pirc, G.; Stare, J. Titanium site preference problem in the TS-1 zeolite catalyst: A periodic Hartree–Fock Study. *Acta Chim. Slov.* **2008**, *55*, 951–959.
- (8) Gale, J. D. A periodic density functional study of the location of titanium within TS-1. *Solid State Sci.* **2006**, *8*, 234–240.
- (9) Ratnasmay, P.; Srinivas, D. Active sites and reactive intermediates in titanium silicate molecular sieves. *Adv. Catal.* **2004**, *48*, 1–169.
- (10) Bordiga, S.; Bonino, F.; Damin, A.; Lamberti, C. Reactivity of Ti(IV) species hosted in TS-1 towards H_2O_2 – H_2O solutions investigated by ab initio cluster and periodic approaches combined with experimental XANES and EXAFS data: A review and new highlights. *Phys. Chem. Chem. Phys.* **2007**, *9*, 4854–4878.
- (11) Bonino, F.; Damin, A.; Ricciardi, G.; Ricci, M.; Spano, G.; D’Aloisio, R.; Zecchina, A.; Lamberti, C.; Prestipino, C.; Bordiga, S. Ti-peroxo species in the TS-1/ H_2O_2 / H_2O system. *J. Phys. Chem. B* **2004**, *108*, 3573–3583.
- (12) Urakawa, A.; Burgi, T.; Skrabal, P.; Bangerter, F.; Baiker, A. Hydroperoxide and allylic alcohol with a single-site homogeneous Ti–Si epoxidation catalyst: A spectroscopic and computational study. *J. Phys. Chem. B* **2005**, *109*, 2212–2221.
- (13) Wells, D. H., Jr.; Delgass, W. N.; Thomson, K. T. Evidence of defect-promoted reactivity for epoxidation of propylene in titaniosilicate (TS-1) catalysts: A DFT study. *J. Am. Chem. Soc.* **2004**, *126*, 2956–2962.
- (14) To, J.; Sokol, A. A.; French, S. A.; Catlow, C. R. A.; Sherwood, P.; van Dam, H. J. J. Formation of heteroatom active sites in zeolites by hydrolysis and inversion. *Angew. Chem., Int. Ed.* **2006**, *45*, 1633–1638.
- (15) Nijhuis, A.; Gardner, T. Q.; Weckhuysen, B. M. Modeling of kinetics and deactivation in the direct epoxidation of propene over gold–titania catalysts. *J. Catal.* **2005**, *236*, 153–163.
- (16) de Visser, S. P.; Kaneti, J.; Neumann, R.; Shaik, S. Fluorinated alcohols enable olefin epoxidation by H_2O_2 : Template catalysis. *J. Org. Chem.* **2003**, *68*, 2903–2912.
- (17) Freceero, M.; Gandolfi, R.; Sarzi-Amadè, M.; Rastelli, A. DFT computational study of the epoxidation of olefins with dioxiranes. *Tetrahedron* **1998**, *54*, 6123–6134.
- (18) Freceero, M.; Gandolfi, R.; Sarzi-Amadè, M.; Rastelli, A. Hydrogen bonding effects in the epoxidation of propenol with dioxiranes. A DFT computational study. *Tetrahedron* **1998**, *54*, 12323–12336.
- (19) Gracia, L.; Sambrano, J. R.; Safont, V. S.; Calatayud, M.; Beltrán, A.; Andrés, J. Theoretical study on the molecular mechanism for the reaction of VO_2^+ with C_2H_4 . *J. Phys. Chem. A* **2003**, *107*, 3107–3120.
- (20) de Visser, S. P.; Oligaro, F.; Sharma, P. K.; Shaik, S. What factors affect the regioselectivity of oxidation by cytochrome P450? A DFT study of allylic hydroxylation and double bond epoxidation in a model reaction. *J. Am. Chem. Soc.* **2002**, *124*, 11809–11826.
- (21) Linic, S.; Barteau, M. A. Construction of a reaction coordinate and a microkinetic model for ethylene epoxidation on silver from DFT calculations and surface science experiments. *J. Catal.* **2003**, *214*, 200–212.
- (22) Crehuet, R.; Anglada, J. M.; Cremer, D.; Bofill, J. M. Reaction modes of carbonyl oxide, dioxirane, and methylenebis(oxy) with ethylene: A new reaction mechanism. *J. Phys. Chem. A* **2002**, *106*, 3917–3929.
- (23) Praprotnik, M.; Hočevá, S.; Hodošek, M.; Penca, M.; Janežič, D. New All-Atom Force Field for Molecular Dynamics Simulation of an AlPO₄-34 Molecular Sieve. *J. Comput. Chem.* **2008**, *29*, 122–129.
- (24) Sherwood, P.; de Vries, A. H.; Guest, M. F.; Schreckenbach, G.; Catlow, C. R. A.; French, S. A.; Sokol, A. A.; Bromley, S. T.; Thiel, W.; Turner, A. J.; Billeter, S.; Terstegen, F.; Thiel, S.; Kendrick, J.; Rogers, S. C.; Casci, J.; Watson, M.; King, F.; Karlsen, E.; voll, M. S.; Fahmi, A.; Schafer, A.; Lennartz, C. QUASI: A general purpose implementation of the QM/MM Approach and its application to problems in catalysis. *THEOCHEM* **2003**, *632*, 1–28.
- (25) Sokol, A. A.; Bromley, S. T.; French, S. A.; Catlow, C. R. A.; Sherwood, P. Hybrid QM/MM embedding approach for the treatment of localized surface states in ionic materials. *Int. J. Quantum Chem.* **2004**, *99*, 695–712.
- (26) Catlow, C. R. A.; French, S. A.; Sokol, A. A.; Thomas, J. M. computational approaches to the determination of active site structures and reaction mechanisms in heterogeneous catalysts. *Phil. Trans. R. Soc. A* **2005**, *363*, 913–936.
- (27) Tuma, C.; Sauer, J. A hybrid MP2/Planewave-DFT scheme for large chemical systems: Proton jumps in zeolites. *Chem. Phys. Lett.* **2004**, *387*, 388–394.
- (28) Fermann, J. T.; Moniz, T.; Kiowski, O.; McIntire, T. J.; Auerbach, S. M.; Vreven, T.; Frisch, M. J. Modeling proton transfer in zeolites: Convergence behavior of embedded and constrained cluster calculations. *J. Chem. Theory Comput.* **2005**, *1*, 1232–1239.
- (29) Wells, D. H., Jr.; Joshi, A. M.; Delgass, W. N.; Thomson, K. T. A quantum chemical study of comparison of various propylene epoxidation mechanisms using H_2O_2 and TS-1 catalyst. *J. Phys. Chem. B* **2006**, *110*, 14627–14639.
- (30) Frisch, M. J.; Trucks, G. W.; Schlegel, H. B.; Scuseria, G. E.; Robb, M. A.; Cheeseman, J. R.; Montgomery, J. A.; Vreven, T.; Kudin, K. N.; Burant, J. C.; Millam, J. M.; Iyengar, S. S.; Tomasi, J.; Barone, V.; Mennucci, B.; Cossi, M.; Scalmani, G.; Rega, N.; Petersson, G. A.; Nakatsuji, H.; Hada, M.; Ehara, M.; Toyota, K.; Fukuda, R.; Hasegawa, J.; Ishida, M.; Nakajima, T.; Honda, Y.; Kitao, O.; Nakai, H.; Klene, M.; Li, X.; Knox, J. E.; Hratchian, H. P.; Cross, J. B.; Adamo, C.; Jaramillo, J.; Gomperts, R.; Stratmann, R. E.; Yazyev, O.; Austin, A. J.; Cammi, R.; Pomelli, C.; Ochterski, J. W.; Ayala, P. Y.; Morokuma, K.; Voth, G. A.; Salvador, P.; Dannenberg, J. J.; Zakrzewski, V. G.; Dapprich, S.; Daniels, A. D.; Strain, M. C.; Farkas, O.; Malick, D. K.; Rabuck, A. D.; Raghavachari, K.; Foresman, J. B.; Ortiz, J. V.; Cui, Q.; Baboul, A. G.; Clifford, S.; Ciosowski, J.; Stefanov, B. B.; Liu, G.; Liashenko, A.; Piskorz, P.; Komaromi, I.; Martin, R. L.; Fox, D. J.; Keith, T.; Al-Laham, M. A.; Peng, C. Y.; Nanayakkara, A.; Challacombe, M.; Gill, P. M. W.; Johnson, B.; Chen, W.; Wong, M. W.; Gonzalez, C.; Pople, J. A. *Gaussian 03*, revision B.03; Gaussian, Inc.: Pittsburgh, PA, 2003.
- (31) Lee, C.; Yang, W.; Parr, R. G. Development of the Colle–Salvetti correlation-energy formula into a functional of the electron density. *Phys. Rev. B* **1988**, *37*, 785–789.
- (32) Becke, A. D. Density-functional thermochemistry. III. The role of exact exchange. *J. Chem. Phys.* **1993**, *98*, 5648–5652.
- (33) Tomasi, J.; Persico, M. Quantum mechanical continuum solvation models. *Chem. Rev.* **2005**, *105*, 2999–3094.
- (34) Reed, A. E.; Weinhold, F. Natural bond orbital analysis of near-Hartree–Fock water dimer. *J. Chem. Phys.* **1983**, *78*, 4066–4073.
- (35) Reed, A. E.; Weinstock, R. B.; Weinhold, F. Natural population analysis. *J. Chem. Phys.* **1985**, *83*, 735–756.
- (36) Redondo, A. W. A.; Goddard, I.; Swarts, C. A.; McGill, T. C. Oxidation of silicon surfaces. *J. Vac. Sci. Technol.* **1981**, *19*, 498–501.
- (37) Devlin, D. Personal communication.
- (38) Svensson, M.; Humbel, S.; Froese, R. D. J.; Matsubara, T.; Sieber, S.; Morokuma, K. ONIOM: A multilayered integrated MO + MM method for geometry optimizations and single point energy predictions. A test for Diels–Alder reactions and $\text{Pt}(\text{P}(t\text{-Bu})_3)_2 + \text{H}_2$ oxidative addition. *J. Phys. Chem.* **1996**, *100*, 19357–19363.
- (39) Rappé, A. K.; Casewit, C. J.; Colwell, K. S.; Goddard III, W. A.; Skiff, W. M. UFF, A full periodic table force field for molecular mechanics and molecular dynamics simulations. *J. Am. Chem. Soc.* **1992**, *114*, 10024–10039.
- (40) Sever, R. R.; Root, T. W. DFT study of solvent coordination effects on titanium-based epoxidation catalysts. Part two: Reactivity of titanium hydroperoxo complexes in ethylene epoxidation. *J. Phys. Chem. B* **2003**, *107*, 4090–4099.
- (41) Munakata, H.; Oumi, Y.; Miyamoto, A. A DFT study on peroxy-complex in titaniosilicate catalyst: Hydrogen peroxide activation on titaniosilicalite-1 catalyst and reaction mechanisms for catalytic olefin epoxidation and for hydroxylamine formation from ammonia. *J. Phys. Chem. B* **2001**, *105*, 3493–3501.
- (42) Lomratsiri, J.; Probst, M.; Limtrakul, J. Structure and adsorption of a basic probe molecule on H-ZSM-5 nanostructured zeolite: An embedded ONIOM study. *J. Mol. Graphics Modell.* **2006**, *25*, 219–225.
- (43) Vayssilov, G. N.; van Santen, R. A. Catalytic activity of titanium silicalites—A DFT study. *J. Catal.* **1998**, *175*, 170–174.